ACSNANO
www.acsnano.org
ARTICLE

# Hydrodynamic Propulsion of Liposomes Electrostatically Attracted to a Lipid Membrane Reveals Size-Dependent Conformational Changes

Seyed R. Tabaei,[†,‡,⊥] Jurriaan J. J. Gillissen,[†,‡,⊥] Stephan Block,[∥] Fredrik Höök,[∥] and Nam-Joon Cho*[,†,‡,§]

[†]School of Materials Science and Engineering, Nanyang Technological University, 50 Nanyang Avenue, 639798, Singapore
[‡]Centre for Biomimetic Sensor Science, Nanyang Technological University, 50 Nanyang Drive, 637553, Singapore
[§]School of Chemical and Biomedical Engineering, Nanyang Technological University, 62 Nanyang Drive, 637459, Singapore
[∥]Department of Applied Physics, Chalmers University of Technology, SE-412 96 Göteborg, Sweden

Supporting Information

**ABSTRACT:** **The efficiency of lipid nanoparticle uptake across cellular membranes is strongly dependent on the very first interaction step. Detailed understanding of this step is in part hampered by the large heterogeneity in the physicochemical properties of lipid nanoparticles, such as liposomes, making conventional ensemble-averaging methods too blunt to address details of this complex process. Here, we contribute a means to explore whether individual liposomes become deformed upon binding to fluid cell-membrane mimics. This was accomplished by using hydrodynamic forces to control the propulsion of nanoscale liposomes electrostatically attracted to a supported lipid bilayer. In this way, the size of individual liposomes could be determined by simultaneously measuring both their individual drift velocity and diffusivity, revealing that for a radius of ∼45 nm, a close agreement with dynamic light scattering data was observed, while larger liposomes (radius ∼75 nm) displayed a significant deformation unless composed of a gel-phase lipid. The relevance of being able to extract this type of information is discussed in the context of membrane fusion and cellular uptake.**

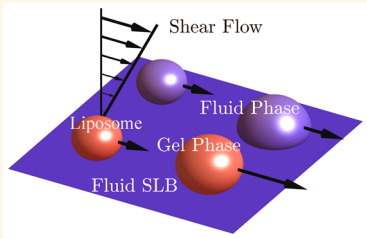


**KEYWORDS:** *liposome deformation, single particle tracking, TIRF microscopy, supported lipid bilayer, hydrodynamic propulsion*

Liposomes (lipid vesicles) are self-closed spherically assembled lipid bilayers, that can be prepared in a size range from around 20 nm up to several $\mu$m.[1,2] Morphologically they resemble cell membranes and other naturally occurring particles such as transport secretory vesicles[3,4] and cell-derived extracellular vesicles,[5] as well as lipid enveloped viruses. Artificial liposomes are widely used as model systems to study membrane-related processes[6] and are more and more frequently used as nanocontainers in drug-delivery applications.[7−9] Many studies reveal a critical influence of liposome size on biological functions, such as enzymatic reaction kinetics,[10,11] protein binding,[12−15] and membrane−protein diffusivity in membranes.[16] The size dependence of the above-mentioned phenomena has been primarily attributed to the stress in a curved membrane, which is related to the area difference of the inner and the outer membrane leaflet, as well as to the mismatch between the physical and spontaneous curvatures.[17,18] As the liposome size is reduced, the curvature increasingly affects the conformations of the molecules that constitute the membrane, leading to changes in both chemical and mechanical properties of the membrane.[12,19−21] It is therefore not surprising that drug encapsulation into liposomes[22] as well as their uptake into cells have been observed to depend on liposome size.[23−27]

Studying the aforementioned size-dependent phenomena is not trivial, though, and requires methods that can independently determine both liposome size and biomolecular content with high accuracy. When freely floating in a liquid, the size can be determined by measuring the diffusivity $D$, which is equivalent, through Einstein's relation $\mu = k_BT/D$, to the friction coefficient $\mu$, where $k_BT$ is the Boltzmann energy, and then by applying the Stokes' drag law, $\mu = 6\pi\eta a$, one can translate the diffusivity $D$ into the radius $a$ *via* the celebrated Stokes−Einstein relation $a = k_BT/6\pi\eta D$. However, when liposomes are in a complex medium, *e.g.*, porous[28,29] or non-Newtonian,[30] or when they are immobilized or moved in a film or on a two-dimensional (2D) interface such as a cellular membrane,[31−35] then Stokes' drag law does not hold and measuring the diffusivity is insufficient to determine the size. In

Received: July 10, 2016
Accepted: August 29, 2016
Published: September 7, 2016






DOI: 10.1021/acsnano.6b04572
ACS Nano 2016, 10, 8812−8820

such cases, one needs to rely on indirect measures of liposome size, by, *e.g.*, correlating lipid content with size,[36] while additional information is required to directly determine the size or changes in size induced upon interactions occurring in complex matrices, *e.g.*, upon binding to a cellular membrane.

We here propose that by combining the above-mentioned diffusion-based determination of the friction coefficient with an independent measurement of the very same parameter both the absolute size and interaction-induced changes in size of membrane-adhering liposomes can be determined. By applying a force $F$ to a particle and measuring the induced drift velocity $U$, which is the steady motion in a fixed direction, as opposed to random diffusive motion, the friction coefficient, $\mu$, can be determined using $\mu = F/U$. If the applied force is a known function of the operating conditions, *e.g.*, radius $a$, drift velocity $U$, *etc.*, then the radius can be obtained by solving

$$F(a, U, ...) = \frac{k_B T U}{D} \quad (1)$$

Alternatively, when the radius is known, then other properties may be extracted from eq 1, such as shape or electric charge. For instance, Yoshina-Ishii *et al.*[37] determined the electrophoretic mobility by measuring the electro-osmotically induced drift velocity and diffusivity of individual negatively charged liposomes, that were tethered using DNA strands to a negatively charged lipid bilayer. Jönsson *et al.*[38] determined the shape of proteins by measuring the shear-induced drift and diffusivity of fluorescently labeled membrane-adhering proteins, while Block *et al.* recently demonstrated that both liposome size and fluorescence emission intensity can be independently determined by using eq 1 in combination with measurements of both $U$ and $D$[39] and that the number of linkers between a liposome and a membrane can be extracted form $D$ alone.[40]

The above-mentioned studies demonstrated the potential of combined diffusivity and drift velocity measurements to extract properties of particles that are confined to a mobile interface but did not specifically address that liposomes may deform in response to interfacial interactions, as previously observed at solid interfaces.[41−46] Inspired by the design of lipid nanoparticles that has been proven efficient in various drug delivery applications, we here apply this approach to determine both the size and conformational changes of individual membrane-adhering liposomes induced by direct membrane−membrane interactions controlled by electrostatic attraction between oppositely charged lipid bilayers in close contact.[47,48] The observed dependence of liposome deformation on size and membrane rigidity is discussed in the context of understanding how to optimize lipid nanoparticle formulations.

## RESULTS AND DISCUSSION

A positively charged supported lipid bilayer (SLB) [PC:EPC (90:10)] was formed using the vesicle fusion method in a fluidic chamber, with width $W$ = 3.8 mm, height $H$ = 0.4 mm, and length $L$ = 17 mm. Negatively charged liposomes (radius $a$ ≈ 45 nm) [PC:PS (95:5)] were fabricated by the extrusion method. After injection into the flow chamber, the liposomes spontaneously adhered electrostatically onto the SLB, where they were observed to diffuse in 2D (see supporting video S1). Prior to injection, the liposome radius distribution was measured using dynamic light scattering (DLS). In Figure 1a, we visualize the diffusive motions of the liposomes by superimposing 350 images taken by fluorescence microscopy, which correspond to a time lapse of 17.5 s. We used particle tracking to reconstruct the liposome trajectories. An example trajectory is displayed in the inset of Figure 1a. To quantify the diffusion, the mean squared displacement (MSD) between all point pairs on the trajectory as a function of the time separation between the paired points was calculated. The MSD in Figure 1b was fitted by eq 6 (see Experimental Section), which gives a diffusivity of $D$ = 0.32 $\mu$m$^2$ s$^{-1}$. Since the trajectory in the inset of Figure 1a, is relatively long, the uncertainty in the fitted $D$ is small (<1%), *i.e.*, the MSD follows eq 6 within 1%. For relatively short trajectories on the other hand, the uncertainty may be larger, and we exclude short trajectories with an uncertainty in the fitted $D$ above 3%.

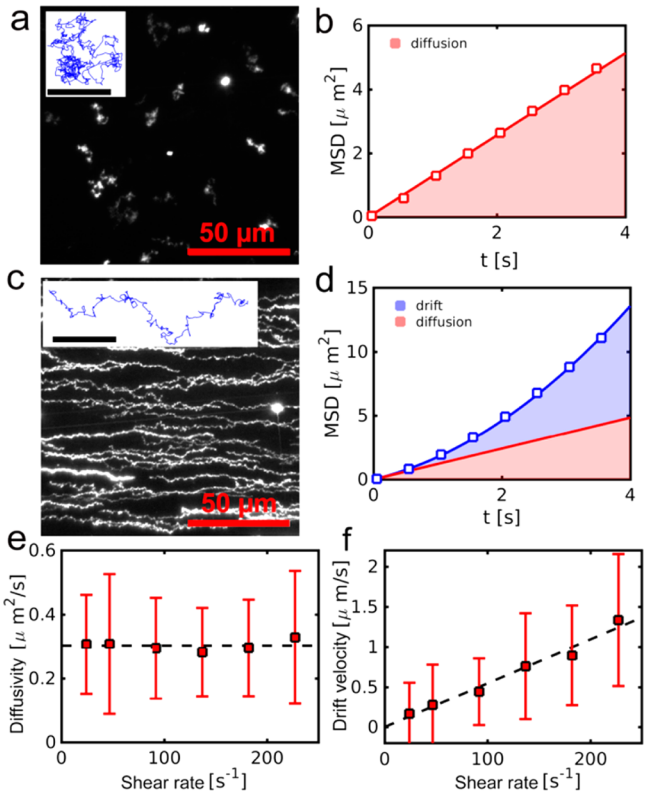


**Figure 1. Liposome motion visualized by the superposition of 350 fluorescence images without applied flow (a) and with applied flow, corresponding to a shear rate of $\gamma$ = 227 s$^{-1}$ (flow rate: $\Phi$ = 23 $\mu$L/s) (c). For each case, a reconstructed trajectory is shown as an inset (the scale bar in the insets corresponds to 5 $\mu$m), and the corresponding mean squared displacements (MSDs) are shown as a function of the elapsed time $t$ in (b) and (d). Without applied flow, the liposome motion is purely diffusive and the MSD is linear (shaded red). With applied flow, the liposome motion includes a substantial drift, reflected by the quadratic part of the MSD (shaded blue). (e) Mean and standard deviation of the diffusivity $D$ as functions of the shear rate $\gamma$. (f) Mean and standard deviation of the drift velocity $U$ as functions of $\gamma$. Note that the data in (e) and (f) are ensemble averaged over all detected trajectories, while the data in (b) and (d) correspond to a single trajectory only.**

Next, aqueous buffer solution was injected into the chamber (see supporting video S2). Figure 1c shows the resulting motion of the membrane-adhering liposomes (volumetric flow velocity: $\Phi$ = 23 $\mu$L/s). The liposome motion was again visualized by overlaying 350 fluorescence images, covering a total time lapse of 17.5 s. The figure shows that in addition to diffusive motion, the particles show a horizontally directed motion (drift). The inset of Figure 1c shows a reconstructed



DOI: 10.1021/acsnano.6b04572
ACS Nano 2016, 10, 8812−8820

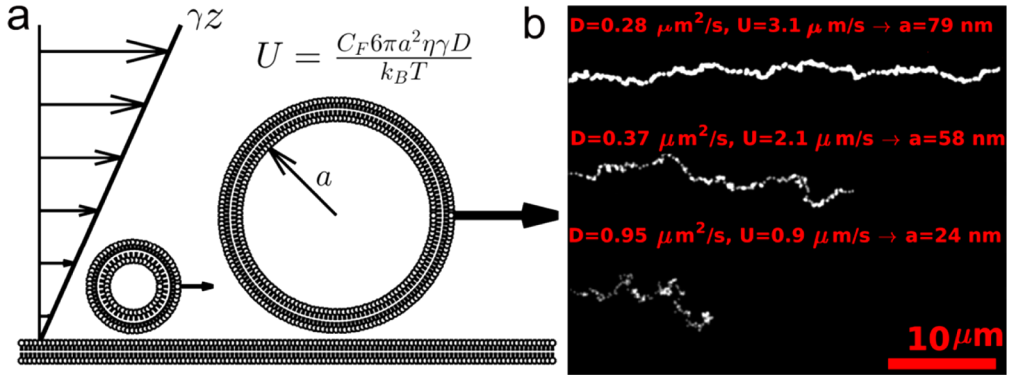


**Figure 2. Illustration of the size-dependent (radius *a*) drift velocity. (a) Cartoon of the shear-induced propulsion of differently sized liposomes. (b) Trajectories, measured with fluorescence microscopy, for three differently sized liposomes. The trajectories are superpositions of diffusion and drift velocity. As the radius of the liposome increases, the drift component increases and the trajectories become less random and more directed.**

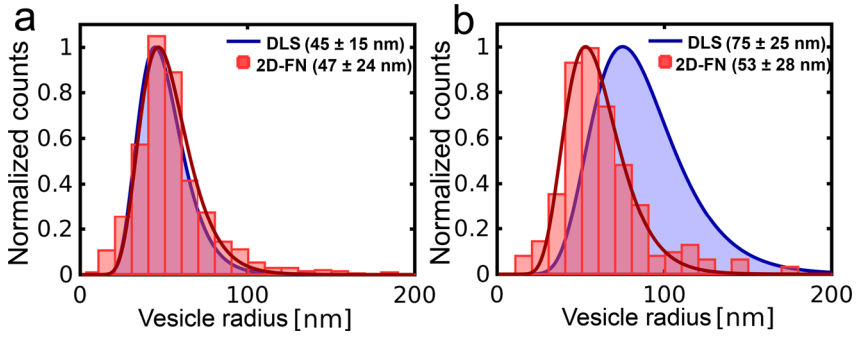


**Figure 3. Radius distribution of membrane-adhering liposomes obtained from 2D flow nanometry [2D-FN, eq 3] (red; bars) and obtained from DLS (blue) (a) for small liposomes (extruded through 100 nm pores) and (b) for large liposomes (extruded through 200 nm pores). The legends indicate the mode and the standard deviation of the respective distributions.**

liposome trajectory, and the corresponding mean squared displacement is shown in Figure 1d. In comparison to the MSD without shear (Figure 1b), the MSD in Figure 1d has an additional, quadratic component, which corresponds to the drift velocity. By fitting eqs 5 and 6 to the data from the trajectory shown in Figure 1d, the drift velocity and diffusivity were determined to be $U = 0.8\ \mu m \cdot s^{-1}$ and $D = 0.25\ \mu m^2 \cdot s^{-1}$, respectively. For the case presented in Figure 1d, the uncertainties in the fitted $U$ and $D$ are small (<1%); *i.e.*, the mean displacement and the mean squared displacement are within 1% of eqs 5 and 6, respectively. Again, it is noted that only sufficiently long trajectories are considered in the analysis such that uncertainties in $U$ and $D$ are below 3%. Following this approach, we determined $U$ and $D$ for about 50 liposome trajectories, reconstructed from the fluorescence image sequence. To study the effect of the flow rate on the diffusivity and on the drift velocity, we repeated the experiment with different flow rates ($\Phi$ between 0 and 23 $\mu L \cdot s^{-1}$).

The fluid velocity experienced by spherical liposomes equals $\gamma a$, where $a$ is the liposome radius and $\gamma$ is the fluid shear rate at the membrane surface, which is the increase of the fluid velocity per unit length when moving away from the surface. The shear rate is related to the flow rate by $\gamma = 6\Phi/WH^2$ and has been varied between 0 and 227 $s^{-1}$ in the present work. In Figure 1e, we observe that changing the shear rate $\gamma$ in this range has no marked effect on the liposome diffusivity, which remains at a constant value of $D = 0.30 \pm 0.1\ \mu m^2 \cdot s^{-1}$. The drift velocity $U$, on the other hand, depends linearly on the shear rate $\gamma$ (Figure 1f). These observations support the view that the friction coefficient between the liposome and the shear flow and the friction coefficient between the liposome and the underlying membrane are both insensitive to the applied shear rate; *i.e.*, they are insensitive to the speed of the liposome.

Now we will use eq 1 to determine the size (radius $a$) of individual membrane-adhering liposomes. To this end, we use the following, generally valid expression, for the shear-induced friction force.

$$F = C_F 6\pi\eta a^2 \gamma \tag{2}$$

Here, $\eta$ is the solvent dynamic viscosity and $C_F$ is the *solvent friction factor*. For solid spheres, $C_F \approx 1.7$,[49] while for other shapes or fluid-like particles, $C_F$ may take on other values. For instance, $C_F$ decreases when the liposome shape deforms from spherical to ellipsoidal under constant area $A = 4\pi a^2$, *i.e.*, with constant effective radius $a$.[38] Therefore, $C_F$ is a measure for the shape of an object, a property that we will exploit later on. Inserting eq 2 into eq 1 results in

$$a = \sqrt{\frac{k_B T U}{C_F 6\pi\eta\gamma D}} \tag{3}$$

For the derivation of eq 3, it has been used that the liposomes move much faster than the SLB, which itself is also being pushed forward by the shear flow, while at the same time, the liposomes move much slower than the fluid; *i.e.*, the friction between the liposomes and the SLB is much larger than the friction between the liposomes and the solvent. A full derivation and a discussion of these assumptions are presented



DOI: 10.1021/acsnano.6b04572
ACS Nano 2016, 10, 8812−8820

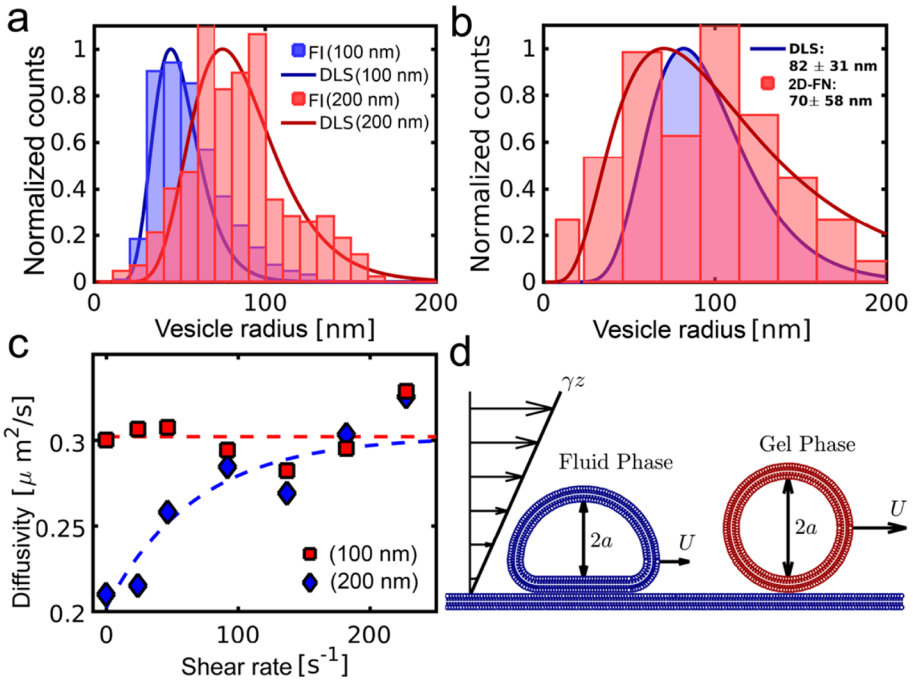


**Figure 4. (a) Radius distribution obtained from the square root of the fluorescence intensity (FI; bars) and obtained from DLS (lines) for small (extruded through 100 nm pores; blue) and large (extruded through 200 nm pores; red) liposomes. (b) Radius distribution for large membrane-adhering, gel phase liposomes, obtained from particle tracking on the membrane interface (eq 3) (red bars) and obtained from DLS (blue). The legends indicate the mode and the standard deviation of the respective distributions. (c) Liposome diffusivity as a function of the shear rate for small liposomes (extruded through 100 nm pores; red squares) and large liposomes (extruded through 200 nm pores; blue diamonds). (d) Schematic representation illustrating that the large fluid-phase liposomes deform and therefore move slower than their undeformed, gel-phase counterparts.**

in the Supporting Information, showing that the SLB moves 100 times slower than the liposomes, which in turn move 10 times slower than the local fluid. Equation 2 suggests that larger particles move faster, since they experience a larger hydrodynamic force from the shear flow (Figure 2a). To illustrate the size-dependent dynamics, we have plotted in Figure 2b the trajectories for three liposomes emitting markedly different fluorescence intensities. For each liposome, the measured diffusivity $D$ and velocity $U$ are given, and the radius $a$, as predicted by eq 3, is seen to correlate well with the observed fluorescence intensity, which is an alternative (control) size measurement, as discussed below. Figure 2b furthermore indicates that with increasing radius the drift velocity increases and the diffusivity decreases, resulting in trajectories that are less random and more directed.

Using the measured drift velocity and diffusivity and assuming that $C_F \approx 1.7$ (solid sphere behavior), eq 3 predicts the radius $a$ of the individual liposomes. We refer to this method as "two dimensional flow nanometry" (2D-FN). The corresponding radius distribution is shown in Figure 3a, where, for the sake of having sufficient statistics, data for all flow rates have been combined. We will discuss the effect of the flow rate on the accuracy of the method below. In Figure 3a, we also plot the radius distribution obtained from dynamic light scattering (DLS). There is nearly perfect agreement between both distributions, which validates that the hydrodynamic interaction between the liposomes and the shear flow resembles that of solid spheres, $C_F \approx 1.7$.

This remarkable observation supports the notions that the small (fluid phase) liposomes (radius ~45 nm) (i) experience a negligible amount of flow in the lipid membrane, *i.e.*, they impose a no-slip boundary condition to the surrounding fluid, similar as for solid particles, and (ii) they do not deform significantly upon adsorption on the membrane surface and remain spherical. The condition of negligible membrane flow is in line with the (successful) use of Stokes' relation (valid for solid spheres) when determining liposome size by measuring the diffusivity.[50] The apparent spherical shape of the adsorbed liposomes implies that the bending energy dominates the substrate-induced adhesion energy.[51] In the literature, liposome deformation has been observed on solid surfaces, suggesting a large substrate-induced adhesion energy (compared to the bending energy).[42,52] Our result of a negligible deformation of small liposomes (radius ~45 nm) on a fluid membrane interface (Figure 3a) suggests that the intermembrane adhesion energy for these liposomes is small compared to the bending energy.

However, with increasing liposome radius $a$, the adhesion energy is expected to increase in proportion to the liposome contact area $\sim a^2$, while the bending energy is independent of $a$.[51,53] Therefore, larger membrane-adhering liposomes are expected to be more prone to shape deformation.[54,55] Such shape deformation would affect the hydrodynamic coupling between the shear flow and the liposome,[38] and to explore this effect, we studied a second batch of larger liposomes (radius $a \approx 75$ nm). Henceforth, we refer to these liposomes ($a \approx 75$ nm) as the "large liposomes", while the ones with $a \approx 45$ nm are referred to as the "small liposomes". Similar to the case of the small liposomes, we measured the drift velocity and the diffusivity of the large liposomes at various shear rates and computed the radii of the individual liposomes using eq 3. The resulting radius distribution together with the corresponding DLS data are shown in Figure 3b. It is seen that the radius of the large liposomes on the membrane surface (measured by



DOI: 10.1021/acsnano.6b04572
*ACS Nano* 2016, 10, 8812–8820

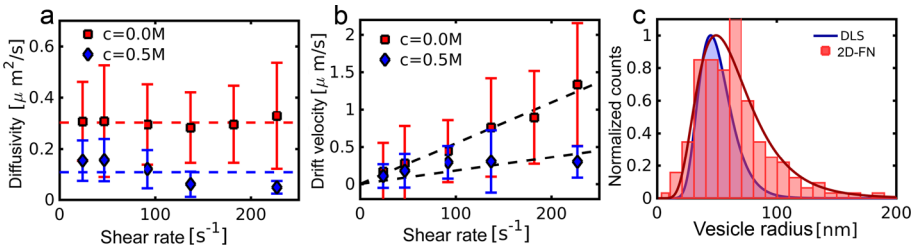


**Figure 5. Effect of glucose on the hydrodynamic propulsion of the small liposomes. (a) Mean (markers) and standard deviation (error bars) of the liposome diffusivity $D$ as functions of the shear rate $\gamma$ with 500 mM glucose in solution (blue diamond) and without glucose in solution (red square). (b) Mean and standard deviation of the liposome drift velocity $U$ as functions of the shear rate $\gamma$ with 500 mM glucose in solution (blue diamond) and without glucose in solution (red square). (c) Radius distribution of membrane-adhering liposomes in 500 mM glucose solution, obtained from 2D-FN (eq 3) (red; bars) and obtained from DLS (blue).**

2D-FN) is smaller than the corresponding values in bulk (measured by DLS). This result indicates that the large liposomes are flattened, resulting in a reduced shear-induced propulsion force, as compared to spherical liposomes (with the same surface area). As an effect, the flattened liposomes move slower than the spherical liposomes and appear to be smaller than their actual size in the "eyes" of 2D-FN.

We verified that the DLS radius distribution, which was measured for suspended liposomes, is representative for the liposome radius distribution on the membrane surface. To this end, we compared the DLS radius distribution to that of the square root of the fluorescence intensity $I^{1/2}$, emitted by individual membrane-adhering liposomes. This quantity is converted to radius, where the conversion factor is found by matching the peak of the $I^{1/2}$ distribution to that of the DLS.[36,56] Figure 4a shows the resulting distributions, where we have used the same conversion factor for both small and large liposomes. The observation that both resulting distributions closely follow the DLS data strongly supports that DLS is representative for the liposomes on the membrane surface and, therefore, suitable to validate the radius distributions obtained using 2D-FN (Figure 3a,b).

We therefore hypothesize that the deviation with regard to radius determination using 2D-FN flow nanometry and DLS observed for large liposomes (Figure 3b) is due to liposome deformation. To confirm this hypothesis, we conducted a control 2D-FN experiment using large liposomes (radius ∼82 nm) composed of DPPC (1,2-dipalmitoyl-*sn*-glycero-3-phosphocholine) with a gel to liquid transition temperature of ∼40 °C[57] and 5 mol % negatively charged DOPS lipids. The bending energy at room temperature of DPPC (∼250 $k_BT$)[58] is 1 order of magnitude larger than that of DOPC (∼25 $k_BT$),[59] and the gel-phase DPPC liposomes are therefore expected to be less prone to deformation. The resulting 2D-FN radius distribution is compared to the corresponding radius distribution obtained from DLS in Figure 4b, which shows a good agreement between both distributions. The peaks of the distributions are within 10 nm of each other. The improved agreement between 2D-FN and DLS when going from fluid-phase (Figure 3b) to gel-phase (Figure 4b) liposomes strongly supports the hypothesis that the deviation between the radius determination made from 2D-FN and DLS (Figure 3b) is due to deformed shapes of the large fluid-phase liposomes.

Deformation of the large liposomes is further supported by the observation that their diffusivity increases with the applied shear rate, as shown in Figure 4c. This observation implies that with increasing liposome velocity there is a reduced friction coefficient between the liposomes and the membrane surface. This effect may be caused by an increase of the intermembrane separation, due to a shear-induced lift force. The shear-induced lift force requires a nonspherical liposome shape;[60] *i.e.*, it vanishes (relative to the drag force) for spheres at small Reynolds numbers $\mathrm{Re} = a^2\gamma/\nu \approx 10^{-6}$,[61] where $\nu$ is the solvent kinematic viscosity. In the Supporting Information, we analyze the relation between the intermembrane separation and the diffusivity of the membrane-adhering liposomes. The analysis shows that a very small increase in the separation (∼0.4 nm) causes a very large increase in the diffusivity (∼50%). This sensitivity toward the intermembrane spacing supports the notion that a shear-induced lift force acts on the large liposomes, resulting in the observed increase in the diffusivity with increasing shear rate (Figure 4c). This, in turn, supports our hypothesis that the large liposomes are deformed since nonsphericity is required to generate a shear-induced lift force. For the small liposomes, on the other hand, the observed diffusivity is independent of the shear rate (Figure 1e), which is consistent with a spherical liposome shape. Figure 4d presents a cartoon to illustrate that the deformation of large, fluid-phase vesicles results in a smaller drift velocity as that of their gel-phase counterparts.

To further study the relationship between the intermembrane friction and the adhesion force, we changed the latter by adding 500 mM glucose to the solvent, which is nonpermeable to the membrane. Due to their relatively large size (1.5 nm), the glucose molecules are expected to be (at least partly) depleted from the (1 nm) intermembrane hydration layer and thus enhance the intermembrane friction due to a depletion force.[37,62] In addition to the depletion force, the glucose molecules also exert an osmotic pressure, which may deform the liposomes. This would also result in an enhanced intermembrane friction through an extended contact area. We used the 2D-FN method to shed light on these processes by probing not only the intermembrane friction, but also liposome deformation, *via* a change in the hydrodynamic radius. For this experiment, we used the small liposomes, which are non-deformed in the absence of glucose (see Figure 3a). Figure 5a shows that in the presence of glucose the small liposomes have a 50% smaller mean diffusivity: $D = 0.16\ \mu\mathrm{m}^2\cdot\mathrm{s}^{-1}$ as compared to the case without glucose, where $D = 0.30\ \mu\mathrm{m}^2\cdot\mathrm{s}^{-1}$. This decrease in diffusivity corresponds to a doubling of the intermembrane friction force, while changes in bulk viscosity (10%) are of minor importance.[63] The larger intermembrane friction is furthermore reflected by a smaller drift velocity, shown in Figure 5b. Despite the substantially larger intermembrane friction, the radius distribution obtained from 2D-FN (eq 3) is still in good agreement with the DLS data



DOI: 10.1021/acsnano.6b04572
*ACS Nano* 2016, 10, 8812–8820

(Figure 5c), which means that the liposomes remain spherical upon addition of 500 mM glucose, and that the observed reduced diffusivity is most likely the effect of an enhanced intermembrane friction due to a depletion force. While large liposomes (radius ~100 nm) are known to shrink upon exposure to a hyperosmotic solution,[64,65] we do not observe osmotic volume change for small liposomes (radius ~45 nm), in agreement with recent investigations.[66]

Finally, we discuss the accuracy of the method. Figure 6a shows (for the small liposomes) that the relative spread in the measured drift velocity $\Delta U/U$ depends inversely on the applied shear rate $\gamma$ for small $\gamma < 100\ s^{-1}$, while for large $\gamma > 100\ s^{-1}$, $\Delta U/U$ approaches a plateau value that is independent of $\gamma$. This observation indicates that $\Delta U/U$ is composed of a stochastic component, which decreases with increasing drift velocity and a material component that is independent of the drift velocity. The material component reflects variations in the liposome radius, *i.e.*, large liposomes move faster than small liposomes, as well as variations in the liposome shape and composition, such as charge or multilamellarity.

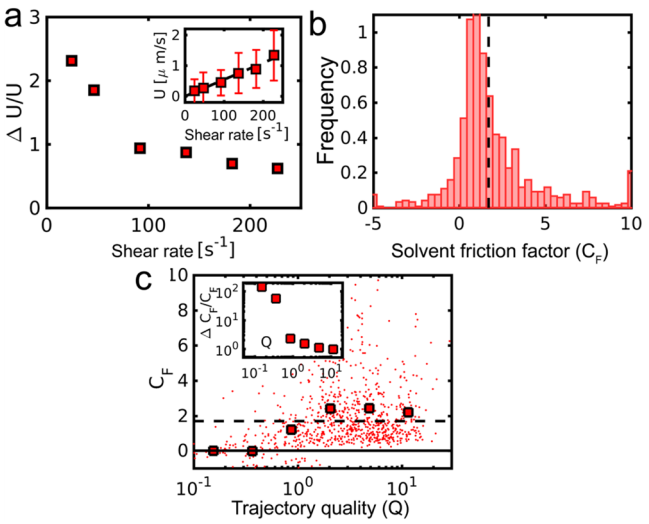


**Figure 6. Accuracy of the 2D flow nanometry (2D-FN) method to determine the radius of the small lipsomes. (a) Relative standard deviation of the liposome drift velocity $U$ as a function of the applied shear rate $\gamma$. The inset shows the liposome drift velocity as a function of the applied shear rate $\gamma$. (b) Distribution of the solvent friction factor: $C_F = k_BTU/(6\pi a^2\eta\gamma D)$. The vertical, dashed line corresponds to the theoretical value for solid spheres: $C_F = 1.7$. (c) Scatter plot of $C_F$ *versus* the trajectory quality: $Q = U(t/D)^{1/2}$. Each dot corresponds to one trajectory. The large markers represent the mean of $C_F$ as a function of $Q$. The inset shows the relative standard deviation of $C_F$ *versus* $Q$.**

To study the accuracy of the method, we compute the solvent friction factor $C_F$ for each individual liposome by inserting the measured values for radius (obtained from fluorescence intensity), diffusivity, and drift velocity into eq 3. While perfect accuracy corresponds to all liposomes giving exactly $C_F = 1.7$, we find a distribution with $C_F = 2.1 \pm 3.9$. Figure 6b shows the corresponding histogram. Despite the large spread, the mean value is surprisingly close to the theoretical value for solid spheres, $C_F = 1.7$. The observed spread is the accumulation of the spread of the depending variables, *i.e.*, liposome radius, diffusivity, and drift velocity $U$. In the Supporting Information, we argue that the measurement uncertainty in the drift velocity $U$, due to the stochastic nature of the diffusion process, is given by $\Delta U/U \approx (D/U^2t)^{1/2}$, which means that the accuracy of the method improves for large values of the so-called trajectory quality $Q$:

$$Q = \sqrt{\frac{U^2 t}{D}} \tag{4}$$

Here, $t$ refers to the total time of the trajectory. We verify this in Figure 6c by showing $C_F$ as a function of $Q$, where each marker corresponds to one trajectory. This figure compiles data for all of the different shear rates. The large markers correspond to the mean $C_F$ as a function of $Q$. This figure shows that for small trajectory quality, $Q \lesssim 1$, the solvent friction factor $C_F$ is distributed around zero, in contrast to the theoretical value of 1.7, while for large trajectory quality, $Q \gtrsim 1$, the mean of $C_F$ approaches the theoretical value of 1.7. The inset of Figure 5c shows the relative standard deviation $\Delta C_F/C_F$, which is a measure for the uncertainty of the present size determination method. The data show that with increasing $Q$ the uncertainty decreases and reaches a plateau value, which supports the notion that for $Q \gtrsim 1$ the uncertainty of the method is no longer governed by the stochastic nature of the diffusion process but rather by deviations in liposome size, shape, and chemical composition. In summary, the successful application of the 2D-FN method requires a sufficiently large flow rate, $Q \gtrsim 1$, to allow an accurate determination of the drift velocity. This requirement must be met under the restrictions of having sufficient ($\gtrsim$100) samples per trajectory to allow tracking of the particle and to ensure an accurate determination of the diffusivity. Additionally, the liposome surface coverage must be sufficiently small, such that individual liposomes can be tracked over the full width of microscopy image. With regard to accuracy, it is further noted that the method is limited to sufficiently large particles, since their velocity must be much larger than the shear-induced velocity of the membrane, such that the latter can be ignored in the analysis. We have shown in the Supporting Information that this condition is met in the current system. For smaller particles, however, such as proteins,[38] this condition will be violated. This problem could be remedied by using anchored lipid bilayers[67] or lipid monolayers on hydrophobic supports.[68]

## CONCLUSIONS

In summary, we have measured the shear-induced drift velocity $U$ and diffusivity $D$ of membrane-adhering liposomes. The radii of the liposomes were determined by combining $U$ and $D$ with the Einstein relation for diffusion under the assumption that the hydrodynamic propulsion force resembles that on solid spheres. For small liposomes (effective radius of ~45 nm), the resulting radius distribution agrees well with DLS measurements, confirming liposome sphericity, while deviations for large fluid phase liposomes (effective radius of ~75 nm) suggest liposome deformation at the membrane interface. The method thus offers a means to measure liposome deformation at a mobile interface, which is particularly relevant in the context of understanding the interaction between liposomes and cellular membranes. In this context, computer simulations of the translocation of nanoparticles across lipid bilayers predicted a better penetrability for elongated particle shapes.[69] In addition, a higher membrane association as well as a faster cellular uptake have been reported for elongated particles in comparison to their spherical counterparts.[70,71] Thus, if we solely consider the



DOI: 10.1021/acsnano.6b04572
ACS Nano 2016, 10, 8812–8820

shape effects, deformation of large liposomes at the membrane interface could promote their cellular entry. On the other hand, lipid exchange and membrane fusion may occur during liposome−cell interactions.[72,73] These processes have been shown to be promoted by increased membrane curvature[74] due to a lowering of the free energy barrier of fusion intermediate structures.[75,76] Thus, liposome deformation at the membrane interface may hinder fusion and inter membrane lipid exchange, which may rather hamper cellular uptake. We thus envision that the approach presented in this work will contribute crucial information that will help unravel the details of these complex processes, which determine the fate of cellular uptake of nanoparticles, in general, and lipid nanoparticles, in particular. Specifically, since nanometer-scale deformations of liposomes and variations in their interaction strength with cellular membranes can be determined for individual liposomes, future studies on cellular uptake of liposomes of different size and rigidity and their interfacial interactions with cell membrane should provide information regarding the importance of shape deformations at the membrane interface for these very often highly heterogeneous systems. This information could thereby serve as design principle for developing more effective liposomal nanocarriers for drug delivery applications. It is also worth noting that although hitherto unique as tool to explore deformation of individual vesicles, AFM will inevitably push the laterally mobile vesicles, which thus risk becoming "invisible". These limitations were here overcome by applying a shear flow, which from optical imaging and single particle tracking made it possible to quantify binding-induced deformation of individual vesicles with sub-10 nm resolution. We thus expect the 2D flow nanometry concept to contribute insight regarding nanoparticle deformation and mapping of the adhesion and binding energies of nanoparticles on mobile interfaces.

## EXPERIMENTAL SECTION

**Liposome Preparation.** Small unilamellar liposomes are fabricated from 1% fluorescently labeled 1,2-dioleoyl-*sn*-glycero-3-phosphoethanolamine-*N*-(lissamine rhodamine B sulfonyl) (rhodamine-PE) lipids, 5% negatively charged 1-palmitoyl-2-oleoyl-*sn*-glycero-3-phospho-L-serine (sodium salt) (DOPS) lipids, and either 94% zwitterionic 1-palmitoyl-2-oleoyl-*sn*-glycero-3-phosphocholine (DOPC) lipids or 94% 1,2-dipalmitoyl-*sn*-glycero-3-phosphocholine (DPPC) lipids by extrusion above the gel to liquid−crystal transition temperature through membranes with either 100 or 200 nm pores. Liposomes are formed in aqueous buffer solution (10 mM Tris (pH 7.5) with 150 mM NaCl).

**SLB Formation and Liposome Adsorption.** Supported lipid bilayers are produced from 10% positively charged 1,2-distearoyl-*sn*-glycero-3-ethylphosphocholine (chloride salt) (DOEPC) lipids and 90% zwitterionic DOPC lipids by the vesicle fusion method on the inner glass wall of a microfluidic channel, with a length $L$, width $W$, and height $H$ of 17, 3.8, and 0.4 mm, respectively. After bilayer formation, liposomes are injected into the channel, which electrostatically adhere to the positively charged supported lipid bilayer, resulting in a relatively low coverage of approximately one liposome per 400 $\mu m^2$, allowing the tracking of individual liposomes. After liposome deposition, the channel is rinsed with buffer solution to eliminate liposomes in the bulk obscuring the subsequent imaging. A hydrodynamic flow is applied to induce drift velocity of the membrane-adhering liposomes. The flow rate is varied from $\Phi$ = 0.84 $mm^3 \cdot s^{-1}$ up to 23 $mm^3 \cdot s^{-1}$, which corresponds to a shear rate from $\gamma = 6\Phi/H^2W$ = 8.3 $s^{-1}$ up to 227 $s^{-1}$.

**Fluorescence Microscopy.** The motion of liposomes on SLBs was observed using a fluorescence microscope with an inverted Eclipse TE 2000 microscope (Nikon) equipped with a high-pressure mercury lamp, a 60× oil objective (NA 1.49), and an Andor iXon+ EMCCD camera (Andor Technology, Belfast, Northern Ireland). The acquired images consisted of 512 × 512 pixels with a pixel size of 0.267 × 0.267 $\mu$m, which is equivalent to an image size of 137 × 137 $\mu$m. During flow, a total of 350 fluorescence images are taken over a period of 17.5 s with a frame rate of 20 $s^{-1}$.

**Liposome Tracking.** In the fluorescence images, liposomes are identified as clusters of more than three and less than 100 pixels whose fluorescence intensities exceeds two times the intensity noise level. Assuming a constant surface number density of the fluorescence molecules within the liposome membranes, the radius of an individual liposome can be estimated from the square root of the fluorescence $I^{1/2}$ emitted by the liposome. The proportionality constant between liposome radius and $I^{1/2}$ is determined by matching the peak of the resulting radius distribution to that obtained from DLS experiments (Malvern Instruments, UK). Liposome positions in subsequent frames are matched to construct liposome trajectories. A trajectory is terminated when the liposome displacement exceeds five pixels or when the liposome comes within five pixels of another liposome. In order to determine liposome diffusivity and drift velocity from the trajectory, we compute for each trajectory the horizontal (flow direction) mean displacement $\overline{\Delta x}$ and the horizontal plus vertical mean squared displacement $\overline{\Delta r^2} = \overline{\Delta x^2} + \overline{\Delta y^2}$ as functions of the elapsed time $t$. For particles moving on a plane, with (horizontal) drift $U$ and diffusivity $D$, these quantities evolve as

$$\overline{\Delta x} = Ut \tag{5}$$

and

$$\overline{\Delta x^2} + \overline{\Delta y^2} = 4Dt + U^2t^2 \tag{6}$$

Measured mean displacement and mean squared displacement are fitted to eqs 5 and 6, which provides the liposome velocity $U$ and diffusivity $D$. In the analysis, we only consider trajectories that are within 3% of the theoretical predictions (eqs 5 and 6). We also ignore liposomes that are stagnant, *i.e.*, when the diffusivity or the velocity is less than 100th of the respective mean value.

## ASSOCIATED CONTENT

### Supporting Information

The Supporting Information is available free of charge on the ACS Publications website at DOI: 10.1021/acsnano.6b04572.

Additional details about the relationships between radius, drift, and diffusivity as well as 2D-FN accuracy; descriptions of videos S1 and S2 (PDF)

Video S1 (AVI)

Video S2 (AVI)

## AUTHOR INFORMATION


### Corresponding Author

*E-mail: njcho@ntu.edu.sg.

### Author Contributions

⊥S.R.T. and J.J.J.G. contributed equally to this work.


### Notes

The authors declare no competing financial interest.

## ACKNOWLEDGMENTS

We gratefully acknowledge support from the National Research Foundation (NRF2015NRF-POC001-019) to N-J.C. and the Swedish Research Council (2014-5557) and Swedish Foundation for Strategic Research (RMA11-0104) 533 to F.H.



DOI: 10.1021/acsnano.6b04572
*ACS Nano* 2016, 10, 8812−8820

## REFERENCES


(1) Cornell, B.; Fletcher, G.; Middlehurst, J.; Separovic, F. The Lower Limit to the Size of Small Sonicated Phospholipid Vesicles. *Biochim. Biophys. Acta, Biomembr.* **1982**, *690*, 15−19.

(2) Walde, P.; Cosentino, K.; Engel, H.; Stano, P. Giant Vesicles: Preparations and Applications. *ChemBioChem* **2010**, *11*, 848−865.

(3) Rizo, J.; Rosenmund, C. Synaptic Vesicle Fusion. *Nat. Struct. Mol. Biol.* **2008**, *15*, 665−674.

(4) Rizzoli, S. O.; Betz, W. J. Synaptic Vesicle Pools. *Nat. Rev. Neurosci.* **2005**, *6*, 57−69.

(5) Fuhrmann, G.; Herrmann, I. K.; Stevens, M. M. Cell-Derived Vesicles for Drug Therapy and Diagnostics: Opportunities and Challenges. *Nano Today* **2015**, *10*, 397−409.

(6) Ostro, M. J. *Liposomes: From Biophysics to Therapeutics*; Marcel Dekker: New York, 1987.

(7) Torchilin, V. P. Recent Advances with Liposomes as Pharmaceutical Carriers. *Nat. Rev. Drug Discovery* **2005**, *4*, 145−160.

(8) Barenholz, Y. Liposome Application: Problems and Prospects. *Curr. Opin. Colloid Interface Sci.* **2001**, *6*, 66−77.

(9) Chatin, B.; Mevel, M.; Devalliere, J.; Dallet, L.; Haudebourg, T.; Peuziat, P.; Colombani, T.; Berchel, M.; Lambert, O.; Edelman, A.; Pitard, B. Liposome-Based Formulation for Intracellular Delivery of Functional Proteins. *Mol. Ther.–Nucleic Acids* **2015**, *4*, e244.

(10) Tabaei, S. R.; Rabe, M.; Zetterberg, H.; Zhdanov, V. P.; Höök, F. Single Lipid Vesicle Assay for Characterizing Single-Enzyme Kinetics of Phospholipid Hydrolysis in a Complex Biological Fluid. *J. Am. Chem. Soc.* **2013**, *135*, 14151−14158.

(11) Rabe, M.; Tabaei, S. R.; Zetterberg, H.; Zhdanov, V. P.; Höök, F. Hydrolysis of a Lipid Membrane by Single Enzyme Molecules: Accurate Determination of Kinetic Parameters. *Angew. Chem., Int. Ed.* **2015**, *54*, 1022−1026.

(12) Hatzakis, N. S.; Bhatia, V. K.; Larsen, J.; Madsen, K. L.; Bolinger, P.-Y.; Kunding, A. H.; Castillo, J.; Gether, U.; Hedegård, P.; Stamou, D. How Curved Membranes Recruit Amphipathic Helices and Protein Anchoring Motifs. *Nat. Chem. Biol.* **2009**, *5*, 835−841.

(13) Tabaei, S. R.; Rabe, M.; Zhdanov, V. P.; Cho, N.-J.; Höök, F. Single Vesicle Analysis Reveals Nanoscale Membrane Curvature Selective Pore Formation in Lipid Membranes by an Antiviral A-Helical Peptide. *Nano Lett.* **2012**, *12*, 5719−5725.

(14) Jackman, J. A.; Saravanan, R.; Zhang, Y.; Tabaei, S. R.; Cho, N. J. Correlation between Membrane Partitioning and Functional Activity in a Single Lipid Vesicle Assay Establishes Design Guidelines for Antiviral Peptides. *Small* **2015**, *11*, 2372−2379.

(15) Tabaei, S. R.; Cho, N. Lamellar Sheet Exfoliation of Single Lipid Vesicles by a Membrane-Active Peptide. *Chem. Commun.* **2015**, *51*, 10272−10275.

(16) Leitenberger, S. M.; Reister-Gottfried, E.; Seifert, U. Curvature Coupling Dependence of Membrane Protein Diffusion Coefficients. *Langmuir* **2008**, *24*, 1254−1261.

(17) Helfrich, W. Elastic Properties of Lipid Bilayers: Theory and Possible Experiments. *Z. Naturforsch. C* **1973**, *28*, 693−703.

(18) Gruner, S. M. Stability of Lyotropic Phases with Curved Interfaces. *J. Phys. Chem.* **1989**, *93*, 7562−7570.

(19) Tian, A.; Capraro, B. R.; Esposito, C.; Baumgart, T. Bending Stiffness Depends on Curvature of Ternary Lipid Mixture Tubular Membranes. *Biophys. J.* **2009**, *97*, 1636−1646.

(20) Seifert, U. Curvature-Induced Lateral Phase Segregation in Two-Component Vesicles. *Phys. Rev. Lett.* **1993**, *70*, 1335.

(21) Oussoren, C.; Zuidema, J.; Crommelin, D.; Storm, G. Lymphatic Uptake and Biodistribution of Liposomes after Subcutaneous Injection.: Ii. Influence of Liposomal Size, Lipid Composition and Lipid Dose. *Biochim. Biophys. Acta, Biomembr.* **1997**, *1328*, 261−272.

(22) Lohse, B.; Bolinger, P.-Y.; Stamou, D. Encapsulation Efficiency Measured on Single Small Unilamellar Vesicles. *J. Am. Chem. Soc.* **2008**, *130*, 14372−14373.

(23) Huang, W.-C.; Burnouf, P.-A.; Su, Y.-C.; Chen, B.-M.; Chuang, K.-H.; Lee, C.-W.; Wei, P.-K.; Cheng, T.-L.; Roffler, S. R. Engineering Chimeric Receptors to Investigate the Size and Rigidity-Dependent Interaction of Pegylated Nanoparticles with Cells. *ACS Nano* **2016**, *10*, 648−662.

(24) Rahman, Y.; Cerny, E.; Patel, K.; Lau, E.; Wright, B. Differential Uptake of Liposomes Varying in Size and Lipid Composition by Parenchymal and Kupffer Cells of Mouse Liver. *Life Sci.* **1982**, *31*, 2061−2071.

(25) Allen, T.; Austin, G.; Chonn, A.; Lin, L.; Lee, K. Uptake of Liposomes by Cultured Mouse Bone Marrow Macrophages: Influence of Liposome Composition and Size. *Biochim. Biophys. Acta, Biomembr.* **1991**, *1061*, 56−64.

(26) Zhang, S.; Gao, H.; Bao, G. Physical Principles of Nanoparticle Cellular Endocytosis. *ACS Nano* **2015**, *9*, 8655−8671.

(27) Yan, Y.; Such, G. K.; Johnston, A. P.; Best, J. P.; Caruso, F. Engineering Particles for Therapeutic Delivery: Prospects and Challenges. *ACS Nano* **2012**, *6*, 3663−3669.

(28) Wang, B.; Anthony, S. M.; Bae, S. C.; Granick, S. Anomalous yet Brownian. *Proc. Natl. Acad. Sci. U. S. A.* **2009**, *106*, 15160−15164.

(29) Wong, I.; Gardel, M.; Reichman, D.; Weeks, E. R.; Valentine, M.; Bausch, A.; Weitz, D. Anomalous Diffusion Probes Microstructure Dynamics of Entangled F-Actin Networks. *Phys. Rev. Lett.* **2004**, *92*, 178101.

(30) Mason, T. G.; Weitz, D. Optical Measurements of Frequency-Dependent Linear Viscoelastic Moduli of Complex Fluids. *Phys. Rev. Lett.* **1995**, *74*, 1250.

(31) Cheung, C.; Hwang, Y.; Wu, X.; Choi, H. Diffusion of Particles in Free-Standing Liquid Films. *Phys. Rev. Lett.* **1996**, *76*, 2531.

(32) Ewers, H.; Smith, A. E.; Sbalzarini, I. F.; Lilie, H.; Koumoutsakos, P.; Helenius, A. Single-Particle Tracking of Murine Polyoma Virus-Like Particles on Live Cells and Artificial Membranes. *Proc. Natl. Acad. Sci. U. S. A.* **2005**, *102*, 15110−15115.

(33) Hormel, T. T.; Kurihara, S. Q.; Brennan, M. K.; Wozniak, M. C.; Parthasarathy, R. Measuring Lipid Membrane Viscosity Using Rotational and Translational Probe Diffusion. *Phys. Rev. Lett.* **2014**, *112*, 188101.

(34) Lee, G. M.; Ishihara, A.; Jacobson, K. A. Direct Observation of Brownian Motion of Lipids in a Membrane. *Proc. Natl. Acad. Sci. U. S. A.* **1991**, *88*, 6274−6278.

(35) Nguyen, Z. H.; Atkinson, M.; Park, C. S.; Maclennan, J.; Glaser, M.; Clark, N. Crossover between 2d and 3d Fluid Dynamics in the Diffusion of Islands in Ultrathin Freely Suspended Smectic Films. *Phys. Rev. Lett.* **2010**, *105*, 268304.

(36) Lohr, C.; Kunding, A. H.; Bhatia, V. K.; Stamou, D. Constructing Size Distributions of Liposomes from Single-Object Fluorescence Measurements. *Methods Enzymol.* **2009**, *465*, 143−160.

(37) Yoshina-Ishii, C.; Boxer, S. G. Controlling Two-Dimensional Tethered Vesicle Motion Using an Electric Field: Interplay of Electrophoresis and Electro-Osmosis. *Langmuir* **2006**, *22*, 2384−2391.

(38) Jönsson, P.; Jönsson, B. Hydrodynamic Forces on Macromolecules Protruding from Lipid Bilayers Due to External Liquid Flows. *Langmuir* **2015**, *31*, 12708−12718.

(39) Block, S.; Fast, B. J.; Lundgren, A.; Zhdanov, V. P.; Höök, F. Two-Dimensional Flow Nanometry of Biological Nanoparticles for Accurate Determination of Their Size and Emission Intensity. *arXiv preprint arXiv:1604.06077* 2016.

(40) Block, S.; Zhdanov, V. P.; Höök, F. Quantification of Multivalent Interactions by Tracking Single Biological Nanoparticle Mobility on a Lipid Membrane. *Nano Lett.* **2016**, *16*, 4382−4390.

(41) Johnson, J. M.; Ha, T.; Chu, S.; Boxer, S. G. Early Steps of Supported Bilayer Formation Probed by Single Vesicle Fluorescence Assays. *Biophys. J.* **2002**, *83*, 3371−3379.

(42) Jackman, J. A.; Špačková, B.; Linardy, E.; Kim, M. C.; Yoon, B. K.; Homola, J.; Cho, N.-J. Nanoplasmonic Ruler to Measure Lipid Vesicle Deformation. *Chem. Commun.* **2016**, *52*, 76−79.

(43) Schönherr, H.; Johnson, J. M.; Lenz, P.; Frank, C. W.; Boxer, S. G. Vesicle Adsorption and Lipid Bilayer Formation on Glass Studied by Atomic Force Microscopy. *Langmuir* **2004**, *20*, 11600−11606.

(44) Hain, N.; Gallego, M.; Reviakine, I. Unraveling Supported Lipid Bilayer Formation Kinetics: Osmotic Effects. *Langmuir* **2013**, *29*, 2282−2288.




DOI: 10.1021/acsnano.6b04572
*ACS Nano* 2016, 10, 8812−8820

(45) Oh, E.; Jackman, J. A.; Yorulmaz, S.; Zhdanov, V. P.; Lee, H.; Cho, N.-J. Contribution of Temperature to Deformation of Adsorbed Vesicles Studied by Nanoplasmonic Biosensing. *Langmuir* **2015**, *31*, 771−781.
(46) Jackman, J. A.; Tabaei, S. R.; Zhao, Z.; Yorulmaz, S.; Cho, N.-J. Self-Assembly Formation of Lipid Bilayer Coatings on Bare Aluminum Oxide: Overcoming the Force of Interfacial Water. *ACS Appl. Mater. Interfaces* **2015**, *7*, 959−968.
(47) Solon, J.; Pécréaux, J.; Girard, P.; Fauré, M.-C.; Prost, J.; Bassereau, P. Negative Tension Induced by Lipid Uptake. *Phys. Rev. Lett.* **2006**, *97*, 098103.
(48) Kunze, A.; Svedhem, S.; Kasemo, B. Lipid Transfer between Charged Supported Lipid Bilayers and Oppositely Charged Vesicles. *Langmuir* **2009**, *25*, 5146−5158.
(49) O'Neill, M. A Sphere in Contact with a Plane Wall in a Slow Linear Shear Flow. *Chem. Eng. Sci.* **1968**, *23*, 1293−1298.
(50) Filipe, V.; Hawe, A.; Jiskoot, W. Critical Evaluation of Nanoparticle Tracking Analysis (Nta) by Nanosight for the Measurement of Nanoparticles and Protein Aggregates. *Pharm. Res.* **2010**, *27*, 796−810.
(51) Lipowsky, R.; Seifert, U. Adhesion of Vesicles and Membranes. *Mol. Cryst. Liq. Cryst.* **1991**, *202*, 17−25.
(52) Reviakine, I.; Gallego, M.; Johannsmann, D.; Tellechea, E. Adsorbed Liposome Deformation Studied with Quartz Crystal Microbalance. *J. Chem. Phys.* **2012**, *136*, 084702.
(53) Seifert, U. Configurations of Fluid Membranes and Vesicles. *Adv. Phys.* **1997**, *46*, 13−137.
(54) Dimitrievski, K. Deformation of Adsorbed Lipid Vesicles as a Function of Vesicle Size. *Langmuir* **2010**, *26*, 3008−3011.
(55) Jackman, J. A.; Zhdanov, V. P.; Cho, N.-J. Nanoplasmonic Biosensing for Soft Matter Adsorption: Kinetics of Lipid Vesicle Attachment and Shape Deformation. *Langmuir* **2014**, *30*, 9494−9503.
(56) Olsson, T.; Zhdanov, V. P.; Höök, F. Total Internal Reflection Fluorescence Microscopy for Determination of Size of Individual Immobilized Vesicles: Theory and Experiment. *J. Appl. Phys.* **2015**, *118*, 064702.
(57) Biltonen, R. L.; Lichtenberg, D. The Use of Differential Scanning Calorimetry as a Tool to Characterize Liposome Preparations. *Chem. Phys. Lipids* **1993**, *64*, 129−142.
(58) Lee, C.-H.; Lin, W.-C.; Wang, J. All-Optical Measurements of the Bending Rigidity of Lipid-Vesicle Membranes across Structural Phase Transitions. *Phys. Rev. E: Stat. Phys., Plasmas, Fluids, Relat. Interdiscip. Top.* **2001**, *64*, 020901.
(59) Pan, J.; Mills, T. T.; Tristram-Nagle, S.; Nagle, J. F. Cholesterol Perturbs Lipid Bilayers Nonuniversally. *Phys. Rev. Lett.* **2008**, *100*, 198103.
(60) Seifert, U. Hydrodynamic Lift on Bound Vesicles. *Phys. Rev. Lett.* **1999**, *83*, 876.
(61) Saffman, P. The Lift on a Small Sphere in a Slow Shear Flow. *J. Fluid Mech.* **1965**, *22*, 385−400.
(62) Asakura, S.; Oosawa, F. On Interaction between Two Bodies Immersed in a Solution of Macromolecules. *J. Chem. Phys.* **1954**, *22*, 1255−1256.
(63) Yoshina-Ishii, C.; Chan, Y.-H. M.; Johnson, J. M.; Kung, L. A.; Lenz, P.; Boxer, S. G. Diffusive Dynamics of Vesicles Tethered to a Fluid Supported Bilayer by Single-Particle Tracking. *Langmuir* **2006**, *22*, 5682−5689.
(64) De Gier, J. Osmotic Behaviour and Permeability Properties of Liposomes. *Chem. Phys. Lipids* **1993**, *64*, 187−196.
(65) Ohlsson, G.; Tabaei, S. R.; Beech, J.; Kvassman, J.; Johanson, U.; Kjellbom, P.; Tegenfeldt, J. O.; Höök, F. Solute Transport on the Sub 100 Ms Scale across the Lipid Bilayer Membrane of Individual Proteoliposomes. *Lab Chip* **2012**, *12*, 4635−4643.
(66) Brändén, M.; Tabaei, S. R.; Fischer, G.; Neutze, R.; Höök, F. Refractive-Index-Based Screening of Membrane-Protein-Mediated Transfer across Biological Membranes. *Biophys. J.* **2010**, *99*, 124−133.
(67) Tanaka, M.; Sackmann, E. Polymer-Supported Membranes as Models of the Cell Surface. *Nature* **2005**, *437*, 656−663.
(68) Plant, A. L. Supported Hybrid Bilayer Membranes as Rugged Cell Membrane Mimics. *Langmuir* **1999**, *15*, 5128−5135.
(69) Yang, K.; Ma, Y.-Q. Computer Simulation of the Translocation of Nanoparticles with Different Shapes across a Lipid Bilayer. *Nat. Nanotechnol.* **2010**, *5*, 579−583.
(70) Tree-Udom, T.; Seemork, J.; Shigyou, K.; Hamada, T.; Sangphech, N.; Palaga, T.; Insin, N.; Pan-In, P.; Wanichwecharungruang, S. Shape Effect on Particle-Lipid Bilayer Membrane Association, Cellular Uptake, and Cytotoxicity. *ACS Appl. Mater. Interfaces* **2015**, *7*, 23993−24000.
(71) Gratton, S. E.; Ropp, P. A.; Pohlhaus, P. D.; Luft, J. C.; Madden, V. J.; Napier, M. E.; DeSimone, J. M. The Effect of Particle Design on Cellular Internalization Pathways. *Proc. Natl. Acad. Sci. U. S. A.* **2008**, *105*, 11613−11618.
(72) Wrobel, I.; Collins, D. Fusion of Cationic Liposomes with Mammalian Cells Occurs after Endocytosis. *Biochim. Biophys. Acta, Biomembr.* **1995**, *1235*, 296−304.
(73) Ewert, K.; Slack, N. L.; Ahmad, A.; Evans, H. M.; Lin, A. J.; Samuel, C. E.; Safinya, C. R. Cationic Lipid-DNA Complexes for Gene Therapy: Understanding the Relationship between Complex Structure and Gene Delivery Pathways at the Molecular Level. *Curr. Med. Chem.* **2004**, *11*, 133−149.
(74) McMahon, H. T.; Kozlov, M. M.; Martens, S. Membrane Curvature in Synaptic Vesicle Fusion and Beyond. *Cell* **2010**, *140*, 601−605.
(75) Kawamoto, S.; Klein, M. L.; Shinoda, W. Coarse-Grained Molecular Dynamics Study of Membrane Fusion: Curvature Effects on Free Energy Barriers Along the Stalk Mechanism. *J. Chem. Phys.* **2015**, *143*, 243112.
(76) Tabaei, S. R.; Gillissen, J.; Vafaei, S.; Groves, J. T.; Cho, N.-J. Size-Dependent, Stochastic Nature of Lipid Exchange between Nano-Vesicles and Model Membranes. *Nanoscale* **2016**, *8*, 13513−13520.


DOI: 10.1021/acsnano.6b04572
*ACS Nano* 2016, 10, 8812−8820